Science of the Total Environment 542 (2016) 629–641

Contents lists available at ScienceDirect

Science of the Total Environment

journal homepage: www.elsevier.com/locate/scitotenv

Efflorescent sulfates from Baia Sprie mining area (Romania) — Acid mine drainage and climatological approach

Andrei Buzatu [a,*], Harald G. Dill [c], Nicolae Buzgar [a], Gheorghe Damian [b], Andreea Elena Maftei [a], Andrei Ionuţ Apopei [a]

[a] "Alexandru Ioan Cuza" University of Iaşi, Department of Geology, 20A Carol I Blv., 700505 Iaşi, Romania
[b] Technical University Cluj Napoca, North University Center of Baia Mare, 62A Dr. Victor Babeş Street, 430083 Baia Mare, Romania
[c] Gottfried Wilhelm Leibniz University, Welfengarten 1 D-30167, Hannover, Germany

HIGHLIGHTS

- Efflorescent salts from mining areas have a great impact on the environment.
- Secondary minerals are influenced by geology, hydrology, biology and climate.
- AMD-precipitates samples were analyzed by XRD, SEM, Raman and NIR spectrometry.
- The dehydration temperatures and intermediate phases were identified.
- A climatological model was obtained on the formation and long-term presence.

GRAPHICAL ABSTRACT

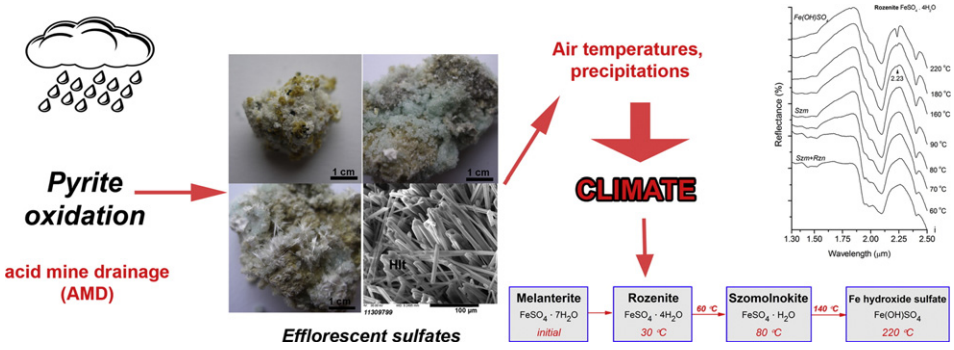

ARTICLE INFO

Article history:
Received 10 September 2015
Received in revised form 16 October 2015
Accepted 27 October 2015
Available online 3 November 2015

Editor: D. Barcelo

Keywords:
Baia Sprie
Acid mine drainage
Ore deposit
Secondary sulfates
Phase transformations
Climate

ABSTRACT

The Baia Sprie epithermal system, a well-known deposit for its impressive mineralogical associations, shows the proper conditions for acid mine drainage and can be considered a general example for affected mining areas around the globe. Efflorescent samples from the abandoned open pit Minei Hill have been analyzed by X-ray diffraction (XRD), scanning electron microscopy (SEM), Raman and near-infrared (NIR) spectrometry. The identified phases represent mostly iron sulfates with different hydration degrees (szomolnokite, rozenite, melanterite, coquimbite, ferricopiapite), Zn and Al sulfates (gunningite, alunogen, halotrichite). The samples were heated at different temperatures in order to establish the phase transformations among the studied sulfates. The dehydration temperatures and intermediate phases upon decomposition were successfully identified for each of mineral phases. Gunningite was the single sulfate that showed no transformations during the heating experiment. All the other sulfates started to dehydrate within the 30–90 °C temperature range. The acid mine drainage is the main cause for sulfates formation, triggered by pyrite oxidation as the major source for the abundant iron sulfates. Based on the dehydration temperatures, the climatological interpretation indicated that melanterite formation and long-term presence is related to continental and temperate climates. Coquimbite and rozenite are attributed also to the dry arid/semi-arid areas, in addition to the above mentioned ones. The more stable sulfates, alunogen, halotrichite, szomolnokite, ferricopiapite and gunningite, can form and persists in all climate regimes, from dry continental to even tropical humid.

* Corresponding author.
E-mail address: andrei.buzatu@uaic.ro (A. Buzatu).

http://dx.doi.org/10.1016/j.scitotenv.2015.10.139
0048-9697/

1. Introduction

The Baia Sprie ore deposit is part of the metallogenetic district of Baia Mare (Fig. 1b). It is located in the NW side of Romania in the inner Neogene volcanic chain of Eastern Carpathians (Fig. 1a). With a tremendous mineralogical association, counting almost 90 mineral species, the Baia Sprie epithermal ore deposit is one of the best-known in Europe. It is the type locality for six minerals: andorite, semseyite, felsobanyaite, dietrichite, klebelsbergite and szmikite (Borcoş et al., 1973; Buzatu et al., 2015; Damian et al., 2003; Manilici et al., 1965; Stanciu, 1973). The deposit consists of a vein system with two major veins: Principal and Southern Veins. The Principal Vein has an impressive length of more than 5 km, 0.5–22 m thickness and more than 800 m depth (Borcoş et al., 1973; Manilici et al., 1965). The mining activity was continuously starting with the 14th century until 2006. It was estimated that up to 1957 approximately 6 million tons of ore was extracted (Manilici et al., 1965). The extraction was done in underground works as well as at the surface, in the Minei Hill open pit, currently abandoned (Fig. 1c). The Baia Sprie mining area shows the proper conditions for acid mine drainage, especially in the Minei Hill open pit, and can be considered a general example for such affected areas on the globe.

The acid mine drainage (AMD) is a major environmental issue all over the world, affecting wide areas where the abandoned or still active mining works are present. A great attention was given to these complex processes of AMD in the recent past (Apopei et al., 2014; Aranda et al., 2012; Bigham and Nordstrom, 2000; Buckby et al., 2003; Buzatu et al., 2012; Joeckel et al., 2005; Majzlan et al., 2011; Schaider et al., 2014; Valente et al., 2013; Valente et al., 2011; Valente and Gomes, 2009; Velasco et al., 2005). When exposed to air and water the geological material is subject to intense weathering which triggers the AMD processes. The sulfides oxidation can lead to acidification of streams and groundwaters and increases the dissolved metal concentrations (depending on the sulfides type, oxidation agents, physical properties and climate factors), with disastrous effects on the environment. One important aspect of AMD is given by the development of newly-formed mineral phases through processes such as oxidation, hydrolysis, neutralization, evaporation (Valente et al., 2013). These minerals consist mainly of efflorescent sulfates with different hydration degrees. Their great impact upon the environment is due to the high solubility, by releasing metals through dissolution during rainfall events (Buckby et al., 2003; Jambor et al., 2000; Joeckel et al., 2005; Valente et al., 2013). The importance of these secondary sulfates in AMD processes relies in their role in controlling pollutants and reflecting the conditions in contaminated areas (Valente et al., 2013; Valente et al., 2011).

Therefore, the understanding of these sulfates behavior is mandatory for such affected areas in mining districts. The structural changes that appear between different phases can offer valuable information regarding the forming-conditions and long-term stabilities. The climatic conditions, such as precipitations, temperature and evaporation, have definitely an important role in formation and presence of AMD-precipitates (Dill et al., 2013). A climatological model regarding the secondary sulfates can help to predict their occurrence in different conditions and to establish the impact of AMD in affected areas on a bigger scale.

This study presents a new approach regarding the climatological conditions in formation and long-term presence in the field of supergene sulfates as products of acid mine drainage in contaminated mining areas. The main goals are: (1) to identify the AMD-precipitates from Baia Sprie mining area and to establish their structural features by means of vibrational spectrometry (Raman and near-infrared); (2) to determine temperatures of phase transformations among these secondary products; (3) to establish the source regarding the acid mine drainage implications; and (4) to address a new interpretation of the formation and stability of secondary sulfates in relation to the climatic conditions on the globe.

2. Geological setting

The Baia Sprie mineralization is an epithermal ore deposit of low-sulfidation type (Damian et al., 2003). It consists of a vein-type system with two main veins: (1) the Principal Vein and (2) Southern Vein, both showing several ramifications towards the upper parts. These veins delimitate an andesitic dyke that is intensive hydrothermally altered in association with the mineralization events (Manilici et al., 1965).

The geology of Baia Sprie area is represented by Tertiary sedimentary rocks mostly covered by Neogene magmatic deposits. Manilici et al. (1965) identified the following igneous rocks: amphibole-pyroxene andesites, rhyolites, quartz-andesites, amphibole-pyroxene dacites, biotite-dacites, and augite-hypersthene basaltic andesites. The amphibole-pyroxene andesites have the greatest distribution being the main rocks that compose Minei Hill area as a 700–1200 m wide block.

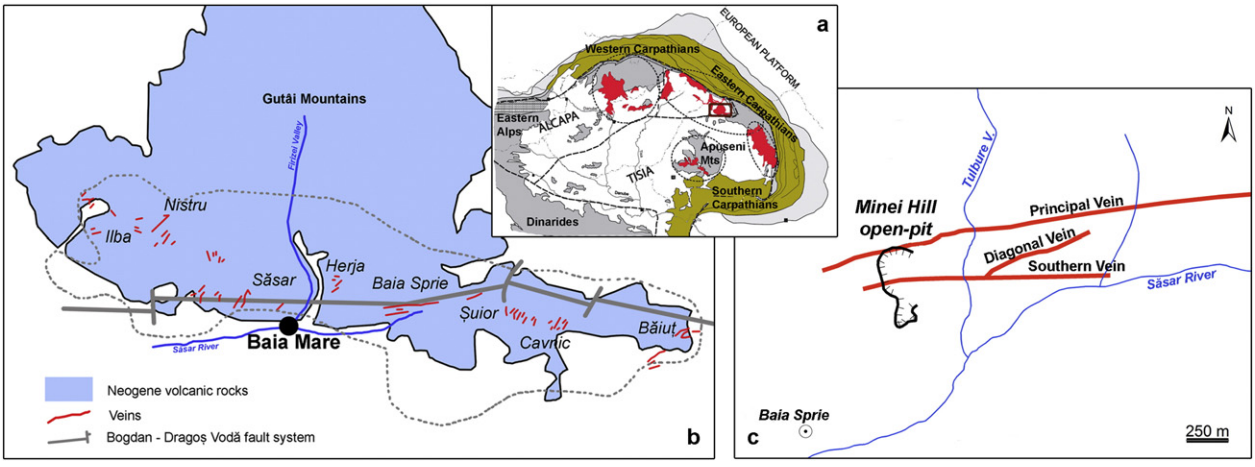

Fig. 1. a. Location of Baia Mare district within the Carpathian-Pannonian region (Seghedi et al., 2004); b. The metallogenetic district of Baia Mare with the main deposits (Grancea et al., 2002); c. Baia Sprie hydrothermal veins and Minei Hill open pit location.

The Baia Sprie mineralization presents a very well-defined vertical zoning, especially within the Principal Vein: the deeper part of the deposit with a copper-rich mineralization, intermediate levels with lead–zinc mineralization, and in the upper parts with gold–silver concentrations (Buzatu et al., 2015; Manilici et al., 1965). The formation of Baia Sprie deposit is considered that it took place in two metallogenetic stages (Borcoş et al., 1973; Buzatu et al., 2015; Manilici et al., 1965). The first one is a cupriferous stage with deposition in the lower part of the deposit. The specific assemblage consists of pyrite, chalcopyrite, magnetite, hematite, scheelite, wolframite, chlorite, quartz, ankerite and barite. The second stage of mineralization has a polymetallic character (Pb–Zn and Au–Ag) and shows occurrences of pyrite, sphalerite, galena, stibnite, tetrahedrite, quartz, calcite and barite. This stage is observed in the intermediate and upper levels of the deposit (Borcoş et al., 1973; Manilici et al., 1965).

Four major types of hydrothermal alteration were observed within Baia Sprie deposit: chlorite, carbonate, adularia and argillic (Stanciu, 1973). The alteration shows a clear zoning with associations between mineralization and alteration zones: Cu ore — chlorite zone; Pb–Zn ore — adularia and carbonate zones; Au–Ag ore — adularia zone (Stanciu, 1973).

The mineralogy of Baia Sprie is quite spectacular, with almost 90 mineral species described, six of which for the first time within this deposit (andorite, semseyite, felsobanyaite, dietrichite, klebelsbergite and szmikite) (Borcoş et al., 1973; Manilici et al., 1965). More recently, new sulfosalts were identified in the upper part of the mineralization, such as freibergite, stephanite and pearceite–polybasite (associated with freibergite, pyrargyrite and miargyrite) (Damian et al., 2003). A new occurrence was described also of several bismuth minerals (bismuthinite, lillianite–gustavite, disordered intergrowths of lillianite homologs, heyrovskyite and cosalite), geocronite–jordanite series and seligmannite member (Buzatu et al., 2015).

The climate regime of the Baia Sprie area is represented by the continental climate zone (type Dfb) according to Köppen–Geiger classification (Koppen, 1936; Peel et al., 2007). The mean annual temperature (from 1961 to 2000) is of 9.5 °C. The warmest months are July and August with a maximum mean temperature of 25 °C. The precipitations are relatively constant during the year, with a mean annual value of 853 mm/year. In the warmest months (July–August) the precipitations reach 195 mm (NMA, 2015). The meteorological data from Romania territory showed significant increases in temperature of ~2 °C, especially during summer, between 1961 and 2007 (NMA, 2015). In the northern part of Romania, the greatest increase in air temperature was observed in June, July and August (Piticar and Ristoiu, 2012). Several studies on climatic changes in Romania have been reported more recently (Croitoru and Piticar, 2013; Croitoru and Piticar, 2014; Croitoru et al., 2015; Dragotă and Kucsicsa, 2011; Dumitrescu and Birsan, 2015). The main results suggest that the climate has become warmer in the last decades at a regional scale in the Carpathians and Intra-Carpathian areas of Romania. Croitoru and Piticar (2013) showed that in the last 50 years the strongest increase was detected for hot extremes such as summer days and tropical nights. In these conditions the aridity increases during the summer, as well as the multi-annual mean temperatures and precipitations in some high mountain areas such as Rodnei Mountains (Dragotă and Kucsicsa, 2011). These preliminary results were confirmed also by Croitoru et al. (2015). Through a detailed analysis of Romania climate in the last 50 years, the authors concluded that the climate become wetter, especially in the northern regions, and the air temperature is increasing.

3. Samples and methods

The studied minerals were observed in the field as efflorescences in complex assemblages resulted from evaporative processes. Several samples of such efflorescent salts were collected from Minei Hill open pit (Fig. 1c). The newly-formed minerals were observed on the exposed walls of the open pit, on the mineralized veins outcrops, and on the ground surface along dried drainage paths (Fig. 2a,b). The primary mineralogy within the open pit area consists of sphalerite, galena, pyrite, chalcopyrite and tetrahedrite, along with gangue minerals such as chlorite, quartz, calcite and barite. These minerals occur in a stockwork structure within the host pyroxene-andesites, which are affected by an intense hydrothermal alteration. The samples were collected in plastic containers and sealed in order to prevent any possible hydration/dehydration of the mineral phases.

From the entire batch a number of 7 final subsamples were obtained by sorting the mineral phases using a binocular magnifier. The sorting was realized by hand-picking considering the color and morphology of crystals in order to achieve as much as possible monomineral samples. The final samples were analyzed using X-ray diffraction (XRD), scanning electron microscopy (SEM), Raman and near-infrared (NIR) spectrometry.

The phases identity in each sample was establish by X-ray powder diffraction using a PANalytical MPD Pro XRD with double detector and Cu anode at 40 kV and with a scan range of 2–85°. The measurements were carried out at the Federal Institute for Geosciences and Natural Resources, Hannover, Germany. The morphology of the minerals was studied using back-scattered electron (BSE) images obtained with a VEGA II LSH scanning electron microscope at an acceleration voltage of 30 kV. The Raman spectra were acquired using a Horiba Jobin-Yvon RPA-HE 532 Raman Spectrograph with a multichannel air cooled CCD detector (−70 °C) and NdYag laser at 532 nm with a nominal power of 100 mW. The spectral range was between 210 and 3400 cm^{-1} with a spectral resolution of 3 cm^{-1}. The Raman system includes a "Superhead" fiber optic Raman probe for non-contact measurements, with a 50× LWD Olympus visible objective. Sulfur and cyclohexane bands were used for the calibration of the frequencies of the Raman spectra. The spectra were acquired using a 2 s exposure time, 30 acquisitions, at a laser power less than 60%, in order to improve the signal-to-noise ratio and to avoid any possible damage of the samples caused by the laser radiation. The spectra were processed using the LabSpec software, through baseline correction and peak fitting (Gaussian + Lorentz).

The near-infrared measurements were carried out using a Portable Infrared Mineral Analyzer (PIMA) from Integrated Spectronics Pty Ltd. The device operates in the 1.3–2.5 μm wavelength region. The radiation penetrates the sample to about 2–3 mm and the measured area is 10 mm in diameter. The spectra were acquired using PimaSP Acquisition v2.1 software and the spectra manipulation was done with PimaView 3.1 package. After an initial set of PIMA analyses was carried out, the samples were treated at different temperatures in order to examine phase transformations and structure changes of every species. Each sample was heated in an electric oven in the 30–90 °C interval of temperature for 4 h for each 10 °C step, and from 100 to 220 °C for 2 h with an increment of 20 °C. After every heating the samples were measured using the PIMA device, therefore obtaining a spectrum for each temperature step showing the dehydration degree and transformations of the mineral phases. The experiment was conducted in ambient air conditions with indoor relative humidity of ~60%. X-ray diffraction measurements were carried out on the final samples in order to identify the phases after the heating process.

4. Vibrational spectrometry of sulfates

The vibrational modes of sulfate minerals are generally classified into three types: (1) vibrations SO_4^{2-} group, (2) H_2O vibrations, and (3) vibrations of cation-oxygen bonds (Nakamoto, 2009). The free sulfate anion in aqueous solution has four fundamental vibrational modes characterized by the following Raman bands: (a) nondegenerate ν_1 symmetric stretching at 981 cm^{-1}, (b) doubly degenerate ν_2 symmetric bending at 451 cm^{-1}, (c) triply degenerate ν_3 antisymmetric stretching at 1104 cm^{-1}, and (d) triply degenerate ν_4 antisymmetric bending at

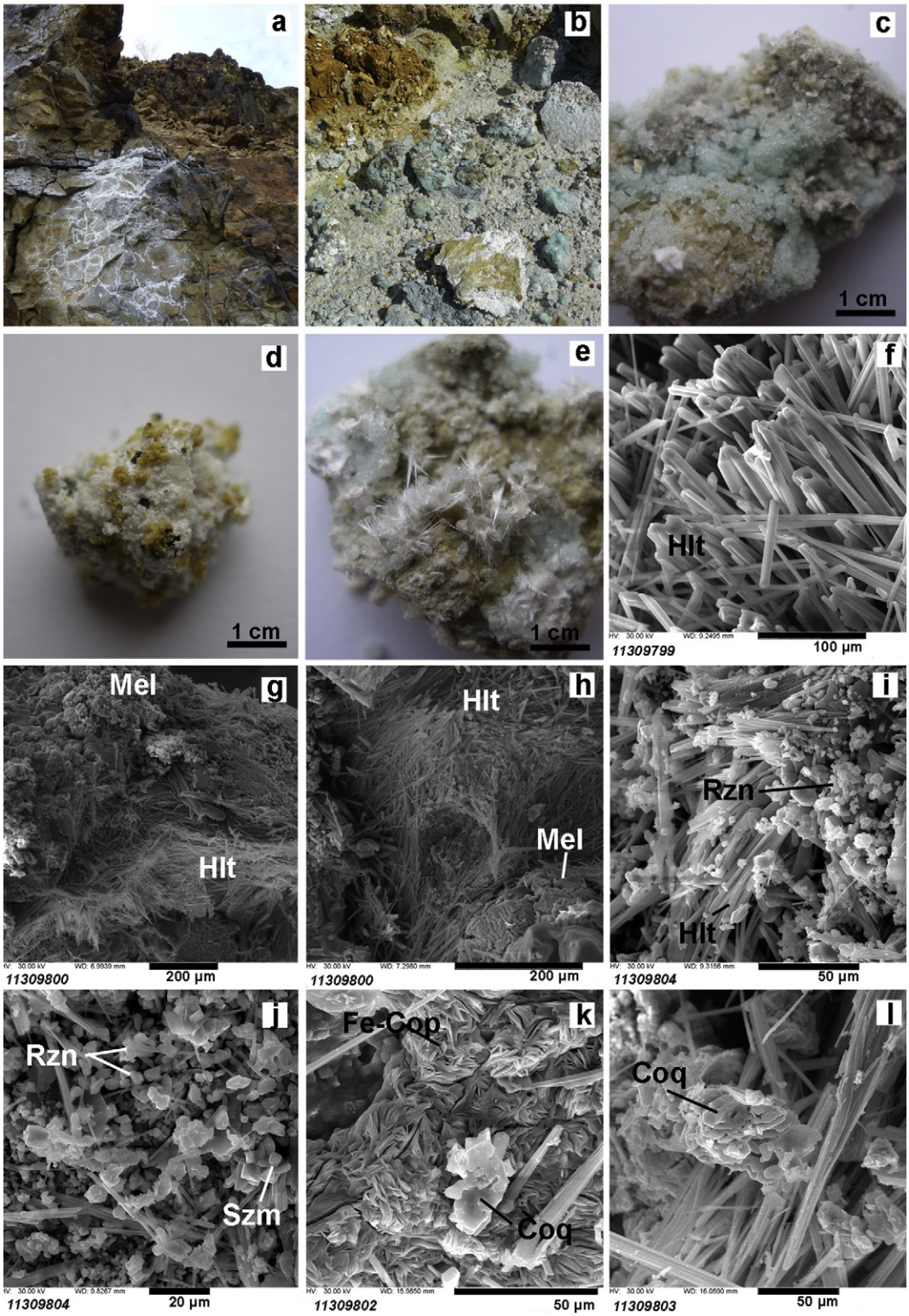

Fig. 2. The occurrence in the field of secondary sulfates and crystal morphologies shown by BSE images. a–b. AMD-precipitates in Minei Hill open pit; c–e. Examples of collected samples consisting in complex associations of secondary sulfates; f. Capillary-acicular habit of halotrichite (Hlt); g–h. Melanterite (Mel) as granular crusts associated with halotrichite; i–j. Rozenite (Rzn) as cotton-like nodules and dipyramidal crystals of szomolnokite (Szm); k–l. Ferricopiapite (Fe-Cop) and coquimbite (Coq) with tabular habit associated with halotrichite.

613 cm^{-1} (Buzgar et al., 2009; Frost et al., 2014; Lane, 2007; Nakamoto, 2009; Omori, 1968). If in solution the SO_4^{2-} group vibrates freely, in minerals the atoms vibrate under additional influences from the cations, reduction in symmetry in the crystal structure causing the splitting of vibrational modes and variation of the bands wavenumber (Buzgar et al., 2009; Nakamoto, 2009; Omori, 1968). The water molecule has the following vibration modes: ν_1 symmetric stretching, ν_2 bending mode, ν_3 antisymmetric stretching, and ν_L libration modes. The stretching modes are observed in the Raman spectra in 3300–3500 cm^{-1} region, and ν_2 bending at 1400–1700 cm^{-1}. The librations appear at ~700–

900 cm^{-1} (Buzgar et al., 2009; Lemus, 2004; Ling and Wang, 2010). The vibration modes M-O can be observed in Raman spectra in the region bellow ~400 cm^{-1}.

The NIR reflectance spectra of sulfate minerals in the range 1.3–2.5 μm can be divided into two sections based on the characteristic bands assignment: (1) the bands between the wavelengths 1.30–1.52 μm are attributed to the first overtone of stretching modes of water (w), $2\nu_1^w$ or $2\nu_3^w$; and (2) the 1.52–2.50 μm region assigned to the combination modes of water $\nu_2^w + \nu_1^w$ (or ν_3^w), and combination modes of water and SO_4 tetrahedra $(\nu_1+\nu_3)^{SO_4}+\nu_2^w$ (Cloutis et al., 2006; Ling and Wang, 2010).

5. Results

5.1. X-ray diffraction

The X-ray diffraction patterns revealed the presence of several AMD-precipitates represented only by sulfates of different metals. The identified sulfates are shown in Table 1. It can be observed that the manual sorting of the efflorescent salts resulted in subsamples that contain just a single major phase, except for samples 11309799 and 11309804, where a mixture of three or two sulfates is present. The identified phases represent mostly iron sulfates with different hydration degrees (szomolnokite, rozenite, melanterite, coquimbite, ferricopiapite), suggesting pyrite oxidation as the main source of AMD-precipitates. Other observed minerals are Zn and Al sulfates (gunningite, alunogen, halotrichite).

The crystal structures of sulfate minerals were well discussed and reviewed by Hawthorne et al. (2000), where a hierarchy was established based on octahedral-tetrahedral units arrangement and polymerization, as follows: (a) isolated polyhedra; (b) finite clusters; (c) infinite chains; (d) infinite sheets; (e) infinite frameworks. Melanterite and alunogen structures consists in isolated SO_4 tetrahedra and MO_6 octahedra linked by direct hydrogen bonds in the case of melanterite, or by interstitial H_2O groups for alunogen. Rozenite, coquimbite and halotrichite are sulfates with finite clusters of polyhedra. Rozenite consists in $M_2(SO_4)O_8$ clusters linked by hydrogen bonds. Coquimbite structure is formed by $M_3(SO_4)_6$ clusters parallel to [001], isolated $Fe^{3+}(H_2O)_6$ octahedra and H_2O groups. The $Fe^{3+}(H_2O)_6$ are connected by hydrogen bonds forming layers of octahedra. Halotrichite consists in finite clusters of $M(SO_4)_2O_4$ polyhedra. The structure of ferricopiapite is formed by infinite $M_2(SO_4)_3O_5$ chains along [101], isolated $M(H_2O)$ and H_2O groups. The most stable structures among the studied sulfates are the ones of szomolnokite and gunningite which are characterized by infinite $M(SO_4)O$ framework of SO_4 tetrahedra and MO_6 octahedra (Hawthorne et al., 2000).

Table 1
The mineralogical composition of the studied samples from Baia Sprie area as obtained through XRD measurements.

Sample	Main minerals	Ideal formula	Space group	Accessory minerals
11309799	Halotrichite	$FeAl_2(SO_4)_4 \cdot 22H_2O$	$P2_1/c$	±Rozenite
	Alunogen	$Al_2(SO_4)_3 \cdot 17H_2O$	$P1$	
	Gunningite	$(Zn,Mn)SO_4 \cdot H_2O$	$C2/c$	
11309800	Melanterite	$FeSO_4 \cdot 7H_2O$	$P2_1/c$	Rozenite
11309801	Halotrichite	$FeAl_2(SO_4)_4 \cdot 22H_2O$	$P2_1/c$	Rozenite ±Melanterite
11309802	Ferricopiapite	$Fe^{3+}{}_{2/3}Fe^{3+}{}_4(SO_4)_6(OH)_2$ $20H_2O$	$P1$	±Coquimbite
11309803	Coquimbite	$Fe^{3+}{}_2(SO_4)_3 \cdot 9H_2O$	$P31c$	Feldspar
11309804	Szomolnokite	$FeSO_4 \cdot H_2O$	$C2/c$	Halotrichite
	Rozenite	$FeSO_4 \cdot 4H_2O$	$P2_1/n$	Gypsum
11309805	Gunningite	$(Zn,Mn)SO_4 \cdot H_2O$	$C2/c$	Nantokite Gypsum ±Starkeyite

5.2. Scanning electron microscopy

The identified efflorescent minerals were observed in complex assemblages of three or more phases. Fig. 2 shows typical modes of occurrence in the field of supergene sulfates and back-scattered electron images (BSE) revealing crystal morphologies in some representative samples. Melanterite was observed as massive granular crusts of bluish green color associated frequently with halotrichite (Fig. 2c, e, g, h). Halotrichite can be easily recognized by its capillary–acicular habit (Fig. 2f). Rozenite and szomolnokite appear commonly in association as cotton-like nodules (rozenite) and dipyramidal crystals (szomolnokite) evolved on the acicular halotrichite (Fig. 2i–j). Ferricopiapite has an intense yellowish-brown color (Fig. 2d) and the crystals form as thin plates intergrowths (Fig. 2k). Coquimbite was observed associated with ferricopiapite and halotrichite showing a tabular-platy habit (Fig. 2k–l).

5.3. Raman and NIR spectrometry

5.3.1. Raman spectrometry

The Raman measurements carried out on the selected subsamples confirmed the XRD results. The sulfate minerals can be easily identified in generally by comparison with reference spectra. The following sulfates were observed: Fe- (melanterite, rozenite, szomolnokite, coquimbite, ferricopiapite), Zn- (gunningite) and Al-sulfates (alunogen, halotrichite). The Raman spectra of the studied sulfates are shown in

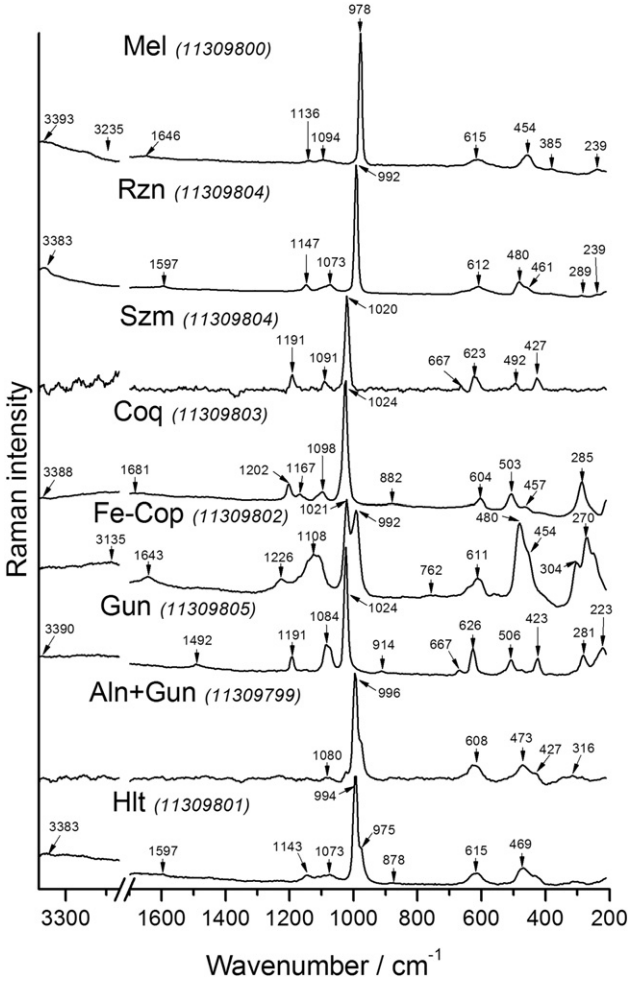

Fig. 3. The Raman spectra of the studied sulfates with the main spectral lines. Melanterite (Mel), rozenite (Roz), szomolnokite (Szm), coquimbite (Coq), ferricopiapite (Fe-cop), gunningite (Gun), alunogen (Aln) and halotrichite (Hlt).

Fig. 3 and the main bands are summarized in Table 2 together with their assignments.

5.3.1.1. Melanterite, rozenite, szomolnokite. The spectra of melanterite, rozenite and szomolnokite from Baia Sprie are dominated by the intense Raman band at 978–1020 cm^{-1} assigned to ν_1 symmetric stretching of SO_4 group (Fig. 3, Table 2). The symmetric bending appears at 385 and 454 cm^{-1} for melanterite, 461 and 480 cm^{-1} for rozenite, 427 and 492 cm^{-1} for szomolnokite. The ν_3 mode is observed at 1136–1191 and 1073–1094 cm^{-1}. The Raman bands at 612, 615, 623 and 667 cm^{-1} are assigned to the antisymmetric bending. The M–O vibration modes appear in the spectra at 239, 273 and 289 cm^{-1}. The water vibration modes are less intense and difficult to distinguish in the obtained spectra. Melanterite and rozenite exhibits stretching modes of H_2O molecules at 3235, 3393 and 3383 cm^{-1} respectively, and bending modes appear at 1646 and 1597 cm^{-1}. None of these three sulfates shows libration modes of H_2O, and szomolnokite presents no water stretching or bending modes either (Table 2).

The comparison of the results with previously reported Raman spectra (Apopei et al., 2014; Apopei et al., 2012; Buzatu et al., 2012; Buzgar et al., 2009; Chio et al., 2005; Chio et al., 2007; Wang and Zhou, 2014) showed a very good agreement of the data and allowed the identification of melanterite, rozenite and szomolnokite in the studied samples from Baia Sprie.

5.3.1.2. Coquimbite, ferricopiapite. The same sulfate characteristics have been observed in the Raman spectra of coquimbite and ferricopiapite where the symmetric stretching mode of SO_4 group appears at 1024 cm^{-1} for coquimbite and 992 and 1021 cm^{-1} for ferricopiapite (Fig. 3, Table 2). The ν_2 vibration mode is observed in the range 412–503 cm^{-1}, and 454–559 cm^{-1}, respectively. The ν_3 and ν_4 antisymmetric modes appear at 1098, 1115, 1167, 1202 and 604 cm^{-1} in the case of coquimbite, and at 1108, 1140, 1226 and 611, 634 cm^{-1} for ferricopiapite. The cation-oxygen vibrations are exhibited in the region bellow 304 cm^{-1}. The H_2O vibration modes are smaller in intensity and can be observed at 3388 and 3135 cm^{-1} — stretching modes; 1681 and 1643 cm^{-1} — bending; 882 and 762 cm^{-1} — librations.

Similar Raman spectra were also reported previously for coquimbite and ferricopiapite (Apopei et al., 2014; Apopei et al., 2012; Frost, 2011; Frost et al., 2014; Kong et al., 2011; Ling and Wang, 2010). Ferricopiapite is a member of copiapite group. This group consists of phases with different cation substitutions (Al^{3+}, Fe^{3+}, Fe^{2+}, Mg^{2+}, Ca^{2+}, Cu^{2+}, Zn^{2+}). The discrimination of ferricopiapite in the present study among the other members of the group was realized based on the work of Frost (2011) and Kong et al. (2011) by taking into consideration the XRD lines and Raman bands.

5.3.1.3. Gunningite. The Raman spectrum of gunningite shows the most intense band at 1024 cm^{-1} assigned to the ν_1 mode of sulfate group (Fig. 3, Table 2). The other modes of SO_4 tetrahedra appear at 423 and 506 cm^{-1} being assigned to the ν_2 mode, 1084 and 1191 cm^{-1} for the antisymmetric stretching, and 626 and 667 cm^{-1} for antisymmetric bending. In the low region of the Raman spectrum, the M–O vibration modes are present at 223 and 281 cm^{-1}. The stretching of water molecule bonds is observed at 3383 cm^{-1}, the bending at 1492 cm^{-1} and the librations appear at 914 cm^{-1}. The obtained Raman results on the samples of gunningite from Baia Sprie are similar with previously reported works, even though few Raman studies have been conducted so far on this mineral (Apopei et al., 2014; Falgayrac et al., 2014; Rudolph et al., 1999).

5.3.1.4. Alunogen, halotrichite. The alunogen and halotrichite Raman spectra are shown in Fig. 3 and the bands values are presented in Table 2. Alunogen was identified at Baia Sprie area just in sample 11309799 which represents a mixture of halotrichite, alunogen and gunningite. Among the vibration modes of SO_4 tetrahedra, the ν_1 symmetric stretching is the most intense at 996 cm^{-1} in the case of alunogen, and 994 and 975 cm^{-1} for halotrichite. The ν_2 bending modes appear at 427, 473 and 431, 469, 525 cm^{-1}. Alunogen shows just one band at 1080 cm^{-1} for the ν_3 mode, while halotrichite shows peaks at 1073, 1110 and 1143 cm^{-1}. The Raman peaks at 608 and 615 cm^{-1} are assigned to the ν_4 antisymmetric bending of SO_4 group. The interactions between the cation and oxygen atoms are indicated by the Raman bands at 314 and 316 cm^{-1}. The presence of water in the crystal structure of alunogen and halotrichite is marked the librations modes at 849 and 878 cm^{-1}. Only halotrichite exhibits the other modes of water molecule at 3383 cm^{-1} — stretching, and 1597–1685 cm^{-1} — bending.

5.3.2. NIR spectrometry

The Portable Infrared Mineral Analyzer (PIMA) operates in the near-infrared (NIR) range between 1.3 and 2.5 μm. In this range are active only minerals that contain certain molecules and ions such as H_2O, OH^-, NH_3, CO_3^{2-}, SO_4^{2-}, and cation-OH bonds (Fe–OH, Al–OH, Mg–OH)

Table 2
The assignment of the main Raman vibration modes of secondary sulfates from Baia Sprie.

	SO_4 vibration modes				H_2O modes			M–O and lattice modes
	ν_1	ν_2	ν_3	ν_4	Stretching	Bending	Librations	
Melanterite	978	385	1094	615	3235	1646		239
		454	1136		3393			
Rozenite	992	461	1073	612	3383	1597		239
		480	1098					289
			1147					
Szomolnokite	1020	427	1091	623				273
		492	1191	667				
Coquimbite	1024	412	1098	604	3388	1681	882	285
		457	1115					
		503	1167					
			1202					
Ferricopiapite	992	454	1108	611	3135	1643	762	250
	1021	480	1140	634				270
		559	1226					304
Gunningite	1024	423	1084	626	3390	1492	914	223
		506	1191	667				281
Alunogen	996	427sh	1080	608sh			849sh	316
		473						
Halotrichite	994	431	1073	615	3383	1597	878	314
	975	469	1110			1685		
		525	1143					

(Bowitz and Ehling, 2008; Cloutis et al., 2006; Velasco et al., 2005). The vibrational modes of these bonds produce diagnostic features at certain wavelengths in the NIR spectra for the minerals that contain them in the crystal structure, making the method suitable for the study of supergene sulfates with different degrees of hydration.

The NIR spectra obtained on the efflorescent sulfates from Baia Sprie are shown in Figs. 4 and 5 and the main bands with their assignments are presented in Table 3. After acquiring the NIR spectra on the initial samples, a heating procedure combined with multiple PIMA analyses were applied, in order to observe the dehydration and structural changes in sulfates at different temperature steps. Figs. 4 and 5 shows selected spectra for each sample at the temperatures where changes were observed. After the final heating temperature (220 °C) the samples were analyzed by XRD to establish the resulted phases of the transformation process.

5.3.2.1. Melanterite, rozenite, szomolnokite. Melanterite was observed in sample 11309800 and the NIR reflectance spectra are shown in Fig. 4. The initial spectrum shows the overtone modes of water at 1.45 and 1.48 μm and the combination modes of water and water–SO_4 at 1.60, 1.97 and 2.40 μm. The diagnostic peak is at 1.97 μm and is observed as a broad and intense band (Fig. 4). During the heating process the NIR spectra reveal changes in sample at the first temperature step (30 °C) where the melanterite changes to rozenite by dehydration with 3 water molecules. The crystal structure changes from isolated polyhedra to finite clusters. Rozenite spectrum shows one band assigned to water overtones at 1.45 μm and multiple ones attributed to the combinations modes at 1.73, 1.95, 1.98 and 2.41 μm. Rozenite structure remains stable up to 60 °C when szomolnokite marks its presence in the NIR spectra. After the heating at 60 °C the sample contains rozenite and szomolnokite, the quantity of rozenite decreasing as the temperature steps increase, as showed by the less and less intense bands of rozenite. At 80 °C rozenite is transformed totally in szomolnokite. The NIR reflectance spectrum of szomolnokite shows the characteristic bands of sulfates at 1.34, 1.44 and 1.52 μm assigned to the overtones of water stretching modes, and at 1.98, 2.09 and 2.40 μm for the combination modes. At 80–90 °C a new peak appears in the NIR spectra at 2.23 μm which increases the intensity towards higher temperature steps

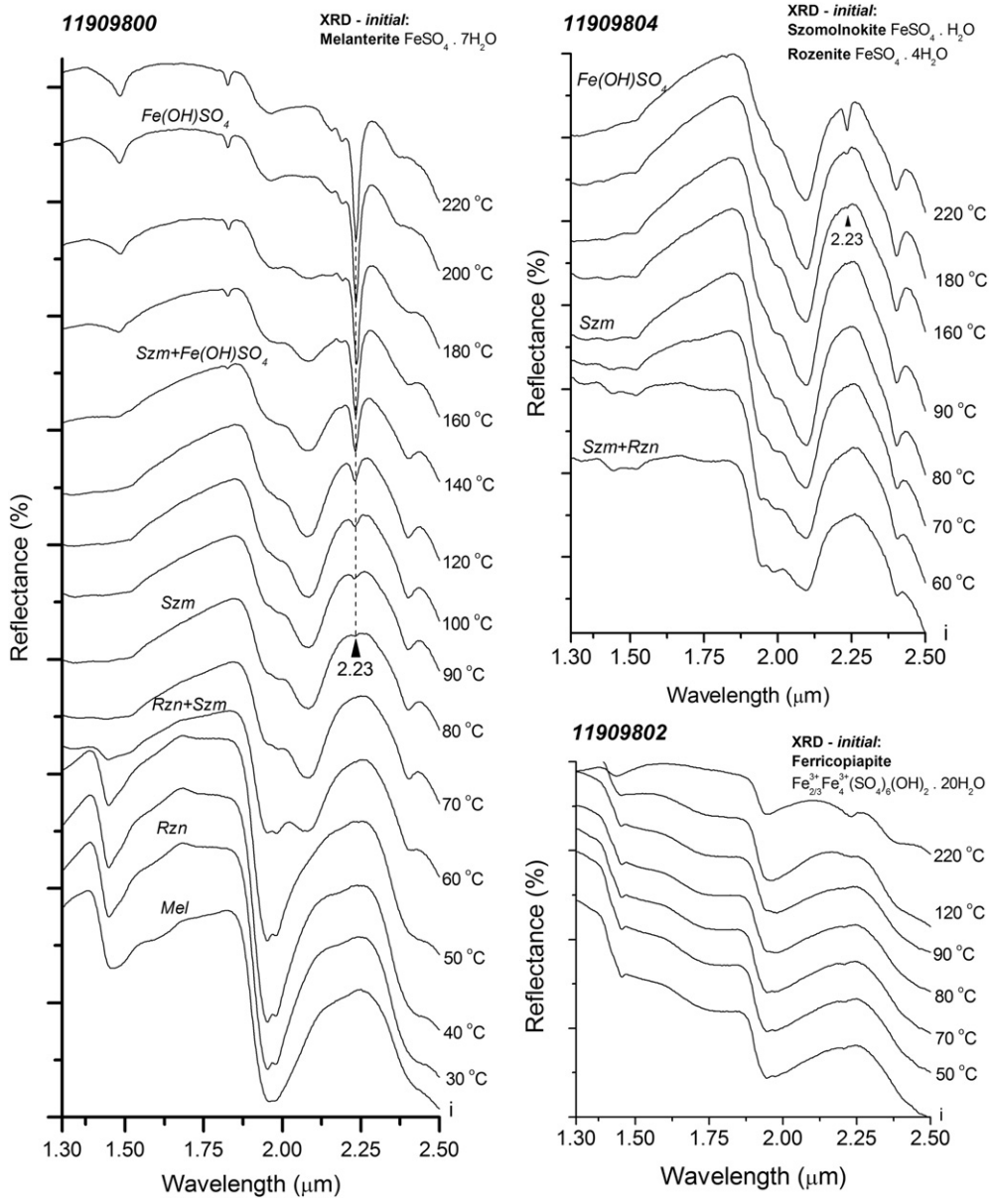

Fig. 4. Selective NIR spectra of samples 11909800, 11909804 and 11908802 at different temperature steps, showing the transformations during the heating procedure. Melanterite (Mel), rozenite (Roz), szomolnokite (Szm).

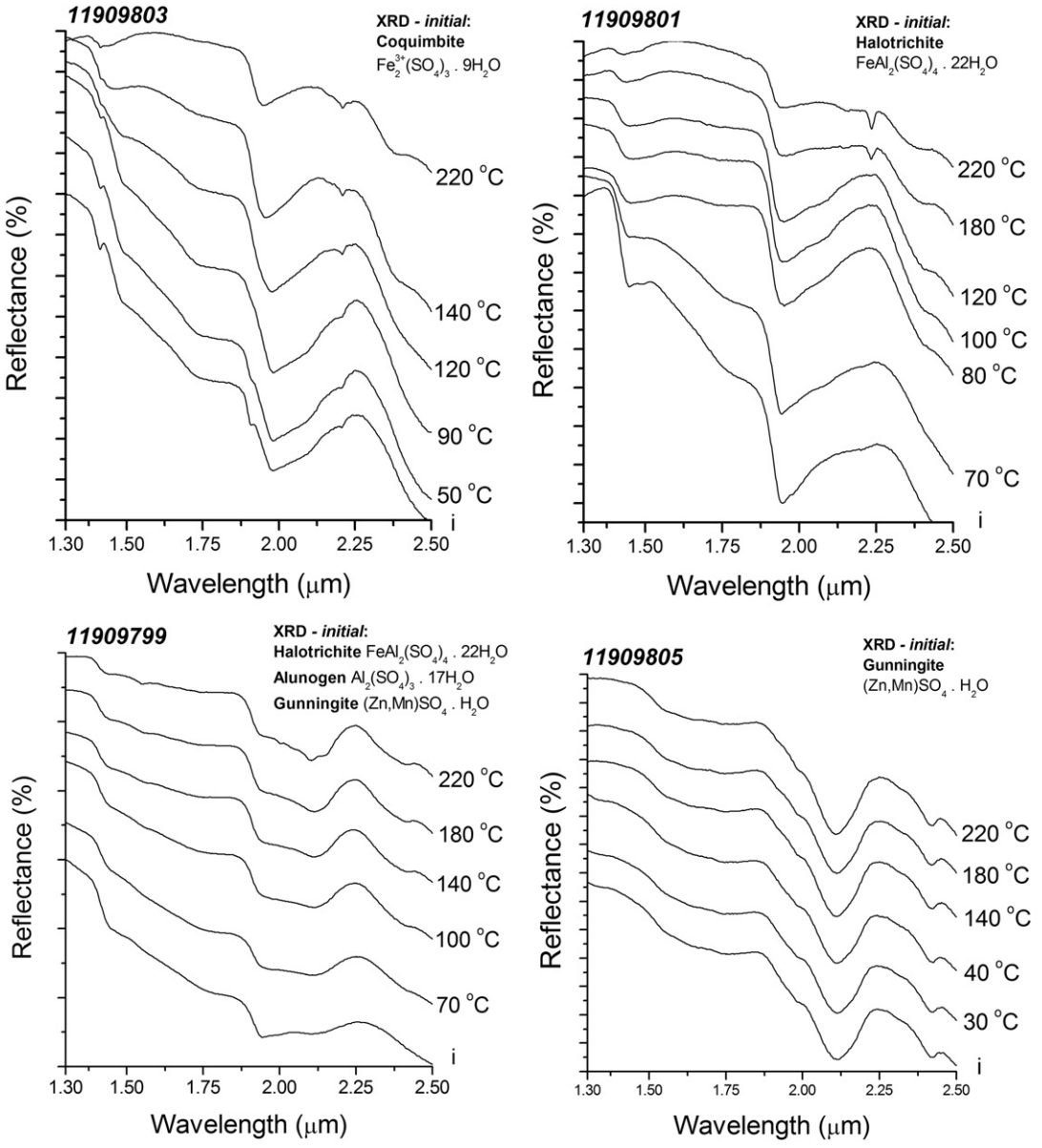

Fig. 5. The NIR spectra of coquimbite, halotrichite, gunningite and alunogen from Baia Sprie at specific temperature steps.

(Fig. 4). At 140 °C other two new peaks are observed at 1.48 and 1.83 μm, while the main band of szomolnokite from 2.09 μm is getting less intense. The new peaks observed at 1.48, 1.83 and 2.23 μm belong to a new compound formed by the dehydration of melanterite, the iron hydroxide sulfate ($Fe(OH)SO_4$). After the final heating at 220 °C the NIR spectrum shows the total transformation of szomolnokite in $Fe(OH)SO_4$, as it was confirmed also by the XRD results.

The sample 11909804 (Fig. 4) which contains szomolnokite and rozenite follows the same transformation pattern by dehydration of rozenite to szomolnokite and iron hydroxide sulfate. The NIR band of $Fe(OH)SO_4$ at 2.23 μm appears in the spectra at 160 °C. At 220 °C the XRD pattern reveals only the presence of szomolnokite in the final sample even though the NIR spectrum shows also the presence of $Fe(OH)SO_4$, but probably in lower amounts. The different behavior of samples 11909800 and 11909804 might be determined by the presence of some impurity minerals in sample 11909804 (Table 1), which did not allowed the total transformation of szomolnokite into iron hydroxide sulfate.

Table 3
The NIR vibration lines of the studied sulfates and their structural assignment.

	Overtone modes of water			Combination modes of water and/or SO_4					
	$2\nu_1^w$ (or $2\nu_3^w$)			$\nu_2^w+\nu_1^w$ (or ν_3^w); $(\nu_1+\nu_3)^{SO_4}+\nu_2^w$					
Melanterite		1.45	1.48	1.60		1.97			2.40
Rozenite		1.45		1.73	1.95	1.98			2.41
Szomolnokite	1.34	1.44	1.52			1.98	2.09		2.40
Coquimbite		1.41	1.48	1.73	1.91	1.98	2.09	2.21	
Ferricopiapite	1.35	1.45		1.76	1.94			2.21	2.42
Gunningite				1.74		1.98	2.11		2.42
Alunogen		1.44			1.94				
Halotrichite		1.45	1.49		1.95	1.98			

5.3.2.2. Coquimbite, ferricopiapite. Sample 11909803 contains coquimbite as major phase as indicated by the XRD pattern. The NIR reflectance spectra are shown in Fig. 5. The characteristic bands of coquimbite appear in the NIR spectrum at 1.41 and 1.48 μm assigned to the overtone modes of water and at 1.73, 1.91, 1.98, 2.09 and 2.21 μm attributed to the combination modes. During the heating it

was observed that the dehydration of coquimbite started at 50 °C when the peak 1.91 μm begins to lower its intensity and it disappears from the spectra at 90 °C. At temperatures of 120–140 °C the most intense peak at 1.98 μm shifts to 1.95 μm and 1.41 μm changes to 1.45 μm. These two new bands show the transformation of coquimbite into mikasaite ($Fe_2^{3+}(SO_4)_3$) based on the NIR results reported by Ling and Wang (2010). Towards higher heating temperatures, the peaks become less intense, indicating the presence of mikasaite in sample at very low concentrations. The XRD pattern of the final sample shows the presence of an amorphous phase. The dehydration of coquimbite was followed by partially transformation into mikasaite and a break-down of the structure into an amorphous phase at temperatures higher than 140 °C.

Ferricopiapite was identified in the sample 11909802. The NIR reflectance spectra are shown in Fig. 4. Ferricopiapite shows the overtone of the stretching modes of water at 1.35 and 1.45 μm and the combination modes of water and SO_4 at 1.76, 1.94, 2.21 and 2.42 μm. The dehydration upon heating is marked in NIR spectra at 90 °C when the band at 1.94 μm starts to get less intense. As in the case of coquimbite, at temperatures of 120–140 °C the main peak in the spectrum becomes 1.95 μm and 1.45 μm slightly shifts to 1.43 μm. The NIR band of $Fe(OH)SO_4$ at 2.23 μm is present in the spectrum but with a very low intensity. The final sample after heating temperature of 220 °C shows very broad and low intensity bands in the NIR spectrum and the XRD pattern revealed the presence of an amorphous phase. This indicates that ferricopiapite dehydrates to $Fe(OH)SO_4$ and mikasaite, which breaks-down at higher temperatures to an amorphous phase.

5.3.2.3. Gunningite. The NIR reflectance spectra of gunningite from sample 11909805 are shown in Fig. 5. The NIR spectrum shows no bands assigned to the overtone modes of water stretching. The combination modes of water and SO_4 are present at the wavelengths 1.74, 1.98, 2.11 and 2.42 μm. Gunningite is the single efflorescent sulfate in this study that showed no changes during the heating procedure. The NIR spectra revealed no modifications in appearance up to 220 °C heating. The XRD measurement on the final sample showed the spectrum of gunningite presenting very clear and sharp characteristic peaks. The crystal structure of gunningite is the most stable among the studied sulfates due to infinite framework of SO_4 and MO_6 polyhedra.

5.3.2.4. Alunogen, halotrichite. Alunogen was observed in sample 11909799 which is a mixture of halotrichite, alunogen and gunningite. The NIR spectra obtained on this sample are shown in Fig. 5. The presence of alunogen is marked by the overtone mode of water at 1.44 μm and combination mode at 1.94 μm. During the heating procedure it was observed a decreasing of the main peaks intensities of alunogen and halotrichite, while the bands of gunningite started to dominate the spectra. After 220 °C the obtained NIR spectra resembles with the one of gunningite, presence of which was confirmed also by the XRD pattern. The absence of other phase in the final sample suggests that alunogen was transform to an amorphous phase starting from 70 to 80 °C (Fig. 5).

Halotrichite was identified as major phase in sample 11909801. The NIR reflectance spectra of halotrichite are shown in Fig. 5. The characteristic bands are observed at 1.45 and 1.49 μm wavelength and are assigned to the overtones of water stretching modes. The most intense peak appears at 1.95 μm with a shoulder at 1.98 μm, both bands being attributed to the combination modes of water and SO_4 tetrahedra. The heating procedure of halotrichite sample showed a continuously decrease of the main peaks intensities up to 120 °C when a new peak is observed at 2.23 μm belonging to iron hydroxide sulfate ($Fe(OH)SO_4$). At 220 °C the 2.23 μm band is more intense suggesting a totally transformation of halotrichite to $Fe(OH)SO_4$ with no intermediate phases, as indicated also by the XRD pattern.

6. Discussion

6.1. Vibrational features and phase transformations

The vibrational spectra of the studied sulfates, both Raman and NIR, were found to be in a good agreement with the typical features of the sulfate minerals, exhibiting the characteristic vibrations, namely the four fundamental vibration modes of the sulfate anion, cation-oxygen modes and water-related vibrations.

One particular vibrational aspect was observed in the Raman spectra of melanterite, rozenite and szomolnokite (Fig. 3). It was noted a shifting trend of the bands assigned to the SO_4 vibration modes towards higher wavenumbers with the decrease of water content. The most clear example is the case of ν_1 mode of SO_4 tetrahedra which is shifting from 978 cm^{-1} in melanterite ($FeSO_4 \cdot 7H_2O$) to 992 cm^{-1} in rozenite ($FeSO_4 \cdot 4H_2O$) and 1020 cm^{-1} in szomolnokite ($FeSO_4 \cdot H_2O$). The structural changes and their effects on the Raman spectra in such hydrous Fe sulfates have been carefully studied previously by other authors (Chio et al., 2005; Chio et al., 2007) who indicated the less extensive H-bonding in the lower hydrates to be the cause of this frequency shifting. The bands position in the Raman spectra are determined by the bond strength. Bonds with greater strength will need higher energies to vibrate, therefore the modes will appear at lower wavenumbers (Buzatu et al., 2013). In the case of Fe sulfates, the crystal structure changes from isolated SO_4 tetrahedra and MO_6 octahedra with complex H-bonding in melanterite, to $M_2(SO_4)O_8$ clusters in rozenite, and finally to an infinite framework of SO_4 and MO_6 polyhedra in szomolnokite (Hawthorne et al., 2000). As the water content decreases the H-bonding becomes less extensive and weaker, the SO_4 ion requiring less energy to vibrate, therefore increasing the vibrational wavenumbers of SO_4 modes (Fig. 3, Table 2).

The phase transformations that occurred during the heating procedure of the studied sulfates, are very well summarized in Fig. 6. All of these phases were established by the NIR spectra acquired at the different temperature steps during the heating, and by XRD measurements on the final samples. The dehydration of melanterite to rozenite at 30 °C was expected as it is known already to be a fast reaction even in low humidity conditions (Chou et al., 2013). Rozenite remains stable until the 60 °C temperature step, when it starts to transform into szomolnokite. The ongoing transformation continues with the iron hydroxide sulfate ($Fe(OH)SO_4$) as a product of szomolnokite dehydration at temperatures of 80–140 °C. The series of decomposition upon heating of these minerals was reported previously to be followed by the formation of mikasaite — $Fe_2^{3+}(SO_4)_3$ at 700 °C, and hematite at 800 °C (Apopei et al., 2014).

Coquimbite and ferricopiapite have both shown a structural breakdown into amorphous phases at temperatures higher than 140 °C, but with mikasaite as an intermediate phase at lower temperatures. In addition, ferricopiapite was observed to transform into a mixture of $Fe(OH)SO_4$ and mikasaite, as suggested by Apopei et al. (2014). The transformation of these two sulfates into mikasaite starts at different temperatures: 50 °C for coquimbite and 90 °C for ferricopiapite. This behavior was reported also by Apopei et al. (2014) in a detailed study on laser irradiation impact on sulfate samples during the Raman measurements, where coquimbite was observed to be slightly more resistant than ferricopiapite: transformation to mikasaite at laser powers on sample surface of 14.3 mW for coquimbite and 18.4 mW for ferricopiapite.

Alunogen and halotrichite were observed to have the same stability temperatures during the heating experiment. At 70 °C both sulfates start to dehydrate. Alunogen transforms into an amorphous phase, while halotrichite changes directly to $Fe(OH)SO_4$ with no intermediate phases.

Gunningite is the only sulfate in this study that showed no changes in the 30–220 °C temperature range. The greater stability of this sulfate relies in the crystalline structure that consists in an infinite framework of SO_4 and MO_6 polyhedra (Hawthorne et al., 2000). Nevertheless,

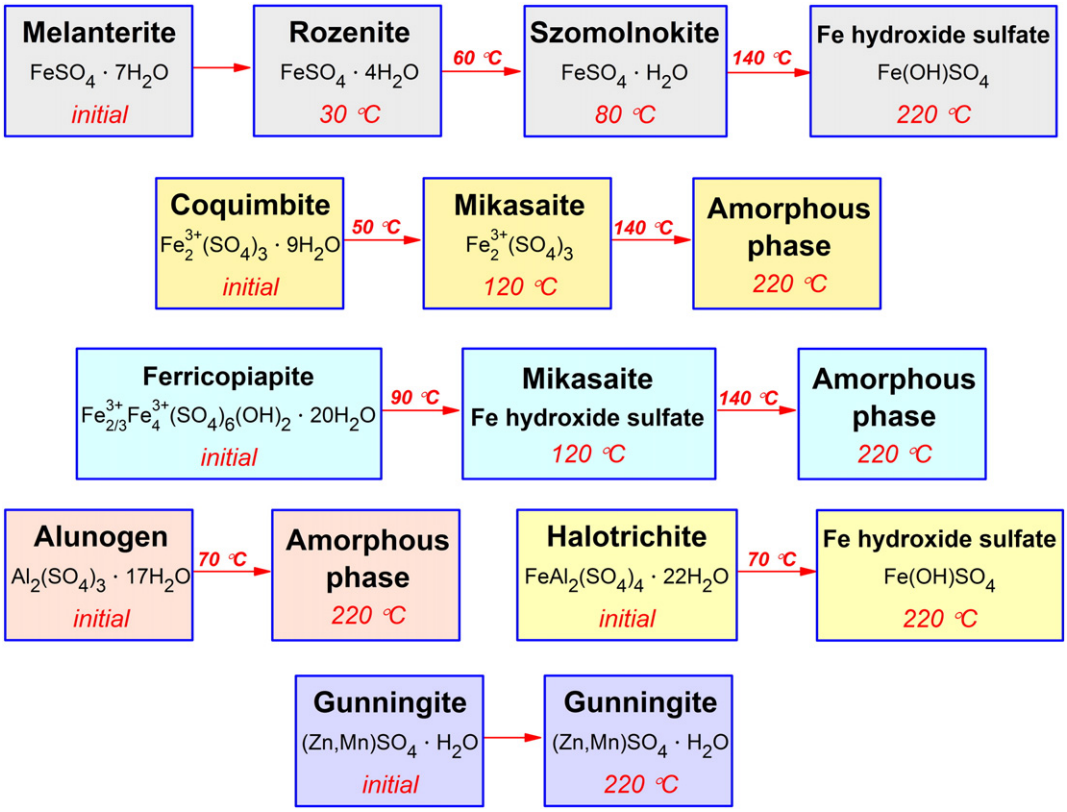

Fig. 6. The phase transformations of the studied sulfates during the heating experiment, with the temperatures of initial dehydration.

gunningite starts to dehydrate at higher temperatures when it transforms into zincosite ($ZnSO_4$) at 400 °C (Apopei et al., 2014).

6.2. Acid mine drainage implications

The above described sulfate minerals are the result of the complex process of acid mine drainage (AMD), caused by the presence of abandoned open pit and underground mining works in the Baia Sprie ore deposit. The AMD is very problematic in such mining districts where the mineralization is affected by supergene alteration. The AMD-precipitates, represented mostly by highly soluble sulfates, are of particular concern since they form during the dry season from sulfate-rich acidic waters, but they will dissolve quickly during the rainfall events (Buckby et al., 2003; Jambor et al., 2000; Joeckel et al., 2005; Valente et al., 2013). This dissolution will cause a spiked increase in dissolved metal concentrations in streams and groundwaters (Jambor et al., 2000). Therefore, it is very important to understand the behavior of these secondary minerals during the AMD process and how the structural transformations among sulfates will enhance the pollution potential of the area.

As it was established so far (Jambor et al., 2000; Valente et al., 2013), the main factors that control the formation of AMD-precipitates are: geology (ore deposit type and host rocks); climate (temperature, precipitations), geography (source distance), hydrology and microbiological activity.

In the Baia Sprie area the precipitations regime is given by two dry periods (mean of 50–60 mm/month) in February–April (lower temperatures) and August–October (higher temperatures), each one being followed by seasonal rainfalls starting with May and November, respectively (maximum mean of 105 mm/month) (NMA, 2015). The samples from this study were collected at the end of June, during the wet period, showing that the observed sulfates are an incipient stage in the formation of AMD-precipitates. The initial stage of sulfates formation is proven also by the presence of melanterite, which has been suggested as the first phase resulted from pyrite oxidation (Buckby et al., 2003; Valente et al., 2013).

The presence of several iron sulfates suggests the pyrite oxidation as the main source of AMD-precipitates from Baia Sprie. The oxidation reactions appear when sulfides (especially pyrite) are exposed to air and moisture (Buckby et al., 2003). The pyrite oxidation is triggered by oxygen leading to a release of Fe^{2+}, SO_4^{2-} and H^+ which lowers the pH (Buckby et al., 2003; Seal et al., 2000).

With the presence of dissolved Fe^{2+} and SO_4^{2-}, the formation of melanterite is straightforward by evaporation and precipitation of the acidic solution. Depending on the temperature and humidity (the quantity of water available), melanterite can dehydrate easily to rozenite and szomolnokite. The sequence melanterite–rozenite–szomolnokite can suggest a decreasing moisture content together with increasing temperature or lower humidity (Buckby et al., 2003; Jambor et al., 2000). Coquimbite and copiapite can precipitate directly from the same type of solutions (Bigham and Nordstrom, 2000; Buckby et al., 2003).

Gunningite formation is based on the sphalerite oxidation which releases and dissolves Zn and SO_4^{2-}. Sphalerite is a main sulfide in the upper part of Baia Sprie ore deposit and it can be observed in large amounts in the Minei Hill open pit (Buzatu et al., 2015). The source of Al for the formation of alunogen and halotrichite is attributed to the breakdown by acidic waters of kaolinite and other clay minerals (mainly aluminosilicates) (Joeckel et al., 2005) from the host rocks, intensively affected by hydrothermal alteration (Buzatu et al., 2015; Stanciu, 1973).

6.3. Climatological approach

The phase transformations outlined in this study for several efflorescent sulfates revealed certain field-stability temperatures for each mineralogical phase. These temperatures can be briefly summarized as indicated in Table 4. The transformation temperatures can be useful to a better and more complete understanding of the behavior of these

Table 4
The secondary sulfates occurrences in AMD environments as function of the climatic zoning.

Sulfates	Mel	Rzn	Szm	Coq	Fe-Cop	Aln	Hlt	Gun
Stable temp. (°C) — this study	<30	<60	<80	<50	<90	<70	<70	<220
Morphoclimatic zones								
Tropical rainforest (humid)								
Central American Cordillera, El Salvador and Bawdin, Myanmar (Dill et al., 2000; Dill et al., 2013 and references therein)					x	x		
Dry arid								
Javier Ortega mine, Peru (Frost et al., 2014)				x	x	x	x	
Temperate humid								
San Miguel mine, Iberian Pyrite Belt, Spain (Velasco et al., 2005)	x	x	x	x	x			
Iron Mountain mine, California, USA (Majzlan et al., 2011)		x	x	x	x		x	
Rio Tinto, Spain (Buckby et al., 2003)	x	x	x	x	x		x	
Dry continental								
Dakota formation, Nebraska, USA (Joeckel et al., 2005)				x	x	x		
Coranda-Hondol, Romania (Apopei et al., 2014)	x	x		x	x			x

Mel — melanterite; Rzn — rozenite; Szm — szomolnokite; Coq — coquimbite; Fe-Cop — ferricopiapite; Aln — alunogen; Hlt — halotrichite; Gun — gunningite.

sulfates, in different forming-conditions, in order to generate a climatological model regarding the formation regime of certain phases. Such an interpretation helps to predict the formation and presence of supergene sulfates in relation to the climate zones and to establish the impact of acid mine drainage in affected areas on a bigger scale. For this, several important aspects have to be considered.

The formation of secondary sulfates through AMD processes is strongly dependent to temperature, precipitations, evaporation rate, and chemical composition of the meteoric fluids (Dill et al., 2013). The chemistry of forming solutions is related to the type of ore deposit, host rocks, and mineralogy on one side, but also with the oxidation and dissolution rates of the primary minerals, mediated and accelerated by micro-bacterial activity (Jambor et al., 2000; Valente et al., 2013).

Considering that the fluids involved in AMD from many examples known in literature, can be generally characterized as acidic sulfate-bearing solutions with different cation contents (Buckby et al., 2003; Jambor et al., 2000; Joeckel et al., 2005), the temperature, precipitation and evaporation remain the variables with an important role in supergene sulfates formation. The changes of these factors are basically defining the climate zoning from pole to equator (Dill et al., 2013; Koppen, 1936; Peel et al., 2007; Summerfield, 1991). The Köppen–Geiger climate classification separates several morphoclimatic zones with increasing temperatures and precipitations from polar to tropical humid zone (Table 5). It is worth mentioning that the weathering depths increase in the same manner, as well as the bacterial activity (Dill et al., 2013).

Another important aspect that should be considered is the ground surface temperature. If the air temperature reaches the highest mean values of 20–30 °C, with maximum extremes of 57 °C (Table 5), the land surface temperatures will be greater, especially in a sun-exposed rocky area in a barren environment such as mining open pits and waste dumps. The ground surface temperature is influenced by several factors (Garratt, 1992; Herb et al., 2008). Mean maximum surface temperatures for soils and asphalt pavements were reported to be in the range of 25–53 °C (Herb et al., 2008; Yilmaz et al., 2008). In the case of extreme temperatures, the direct measurements recorded values of ~80 °C (at air temperature of ~40 °C) for desert areas, and 69 °C (air temperature of 43 °C) for soil covers (Garratt, 1992). Simulation models predict a possible upper limit to the maximum ground surface temperature of 93 °C, in the case of the extreme air temperature ever observed of 57 °C (Garratt, 1992).

With all of these in mind, the stable temperatures of secondary sulfates observed in this study, suggest specific climatic regime for certain phases, that predicts the probability of formation in various areas of the globe. Melanterite has proven to be the most unstable sulfate regarding the ambient temperature (<30 °C), therefore its formation and persistence are constrained to dry continental and temperate humid climate zones, where the mean temperatures are low and humidity is relatively high. Melanterite resistance is less likely in the other climate zones, especially in arid and semi-arid areas where the humidity is very low and the temperature is high. Even for the tropical climate, with increased humidity, iron sulfate will rather form as rozenite or szomolnokite due to the higher temperatures. Coquimbite and rozenite are the following sulfates in temperature stability series (<50–60 °C). These sulfates are attributed to dry arid and semi-arid zones, in addition to the above mentioned ones for melanterite. In these areas the ground surface temperatures will rarely exceed 60 °C, except in case of extreme air temperatures (quite likely due to the low humidity). Alunogen, halotrichite, szomolnokite and ferricopiapite have shown stability temperatures between 70 and 90 °C, which place them in all climate regimes, from dry continental to even tropical humid, since their dehydration starts at higher temperatures. Gunningite has shown no modifications during the heating treatment, its presence being possible in all climates. The primarily condition for gunningite formation remains the Zn availability having as source the sphalerite oxidation.

Table 5
The morphoclimatic zones according to the Köppen–Geiger climate classification, with the values of temperatures and precipitations (Dill et al., 2013; Summerfield, 1991).

Morphoclimatic zones	Mean annual temperature (°C)	Precipitations (mm)	Maximum temperatures (°C)	Average relative humidity (%)
Tropical rainforest (humid)	20–30	>1500	36–38	84.2
Tropical wet–dry	20–30	600–1500	39–42	73–75
Dry semi-arid	10–30	300–600	41–43	39–54
Dry arid	10–30	0–300	41–57	36–41
Temperate humid	0–20	400–1800	36–43	71–78
Dry continental	0–10	100–400	33–40	57–73
Polar and alpine	<0	0–1000	Variable	Variable

This occurrence pattern of AMD-precipitates according to climate has been already reported but not yet highlighted (Table 4). The more stable sulfates (ferricopiapite, alunogen, halotrichite) were identified mostly in arid/semi-arid and tropical conditions, while melanterite, coquimbite, rozenite occur predominantly in continental and temperate climates (Table 4).

Certainly, the relative humidity plays an important role in sulfates stability. The strongest impact should be considered in dry arid/semi-arid zones where the precipitations and humidity are low and it could lead to the dehydration of sulfates, even at lower temperatures than those found as stability limits. This experiment was conducted at a relative humidity of ~60%, which is close even to the average value of tropical wet-dry climate. These should be general rules regarding the long-term presence of efflorescent sulfates, since only mean values were considered on global scale, but temperatures and precipitations are variable/seasonable in all climate zones.

7. Conclusions

The mineralogical study of efflorescent sulfates from Baia Sprie open pit provides an useful insight regarding the phase transformations and structural changes among several sulfates, which allows a better understanding of the acid mine drainage processes in similar affected areas around the globe. Moreover, the experimental results indicate the sulfates behavior in different conditions that helps to predict their formation and long-term presence in relation to the climate zones. This climatological interpretation represents a new approach in the field of acid mine drainage and secondary sulfates genesis.

The vibrational results of the studied sulfates (Raman and NIR) were in a good agreement with the typical features, showing the characteristic vibrations, such as the four fundamental vibrations of sulfate group, cation-oxygen modes and water-related vibrations. The dehydration temperatures and intermediate phases upon decomposition were successfully established for each mineral phase. The melanterite to rozenite (30 °C) to szomolnokite (60 °C) reaction was followed by the transformation to $Fe(OH)SO_4$ at 140 °C. The structures of coquimbite and ferricopiapite have shown breakdowns into amorphous phases at 140 °C with mikasaite ± $Fe(OH)SO_4$ as intermediate phases. Alunogen and halotrichite start to dehydrate at 70 °C and turn amorphous, and into iron hydroxide sulfate, respectively. Gunningite was the single sulfate that showed no transformations in the 30–220 °C temperature range.

The acid mine drainage is the main cause for sulfates formation, triggered by pyrite oxidation as the major source for the abundant iron sulfates. The high amount of sphalerite from the upper part of the Baia Sprie deposit has a fundamental contribution to the formation of gunningite. The Al source for alunogen and halotrichite relies in the dissolution by acidic waters of the hydrothermally altered host rocks. The sulfate precipitation proved to be at an initial stage, as suggested by the presence of melanterite, being the first phase of pyrite oxidation. The sequence melanterite-rozenite-szomolnokite indicates a humidity decreasing together with increasing temperatures during the sampling period.

Since the studied efflorescent sulfates represent minerals of neoformation, it was outlined that the climatic conditions are essential in their precipitation. The climatological interpretation showed that the melanterite formation and presence is strictly related to continental and temperate climates, based on the stability temperatures within this study. Coquimbite and rozenite are attributed also to the dry arid/semi-arid areas, in addition to the above mentioned ones. The more stable sulfates, alunogen, halotrichite, szomolnokite, ferricopiapite and gunningite, can form and persists in all climate regimes, from dry continental to even tropical humid. Nevertheless, these rules should be considered general on a global scale, since the climatic conditions are very variable in the specified zones.

Acknowledgments

We thank D. Weck from Federal Institute for Geosciences and Natural Resources, Hannover, Germany, who carried out the XRD analyses. We are grateful also to dr. Irina Gostin (Alexandru Ioan Cuza University of Iasi, Romania) for providing the scanning electron images. We extend our gratitude to the anonymous reviewers for their time spent reading the manuscript and for the valuable suggestions, as well as to the associate editor Dr. Filip Tack, for the editorial handling of the manuscript.

References

Apopei, A.I., Damian, G., Buzgar, N., 2012. A preliminary Raman and FT-IR spectroscopic study of secondary hydrated sulfate minerals from the Hondol open pit (Metaliferi Mts., Romania). Rom. J. Miner. Depos. 85, 1–6.

Apopei, A.I., Buzgar, N., Damian, G., Buzatu, A., 2014. The Raman study of weathering minerals from the Coranda-Hondol Open Pit (Certej Gold-Silver Deposit) and their photochemical degradation products under laser irradiation. Can. Mineral. 52, 1027–1038.

Aranda, S., Borrok, D.M., Wanty, R.B., Balistrieri, L.S., 2012. Zinc isotope investigation of surface and pore waters in a mountain watershed impacted by acid rock drainage. Sci. Total Environ. 420, 202–213.

Bigham, J.M., Nordstrom, D.K., 2000. Iron and aluminum hydroxysulfates from acid sulfate waters, in: Alpers, C.N., Jambor, J.L., Nordstrom, D.K. (Eds.), Sulfate Minerals — Crystallography, Geochemistry, and Environmental Significance. Reviews in Mineralogy and Geochemistry, Mineralogical Society of America and Geochemical Society, Washington, pp. 351–404.

Borcoş, M., Lang, B., Boştinescu, S., Mîndroiu, V., Volanschi, E., 1973. Considerations regarding metalogenetic activity associated with Pontiene pyroxene andesites from Gutai Mountains (in Romanian). Institutul Geologic, Studii tehnice şi economice Sept, 109.

Bowitz, J., Ehling, A., 2008. Non-destructive infrared analyses: a method for provenance analyses of sandstones. Environ. Geol. 56, 623–630.

Buckby, T., Black, S., Coleman, M.L., Hodson, M.E., 2003. Fe-sulphate-rich evaporative mineral precipitates from the Rio Tinto, southwest Spain. Mineral. Mag. 67, 263–278.

Buzatu, A., Damian, G., Buzgar, N., 2012. Raman and infrared studies of weathering products from Baia Sprie ore deposit (Romania). Rom. J. Miner. Depos. 85, 7–10.

Buzatu, A., Buzgar, N., Damian, G., Vasilache, V., Apopei, A.I., 2013. The determination of the Fe content in natural sphalerites by means of Raman spectroscopy. Vib. Spectrosc. 68, 220–224.

Buzatu, A., Damian, G., Dill, H.G., Buzgar, N., Apopei, A.I., 2015. Mineralogy and geochemistry of sulfosalts from Baia Sprie ore deposit (Romania) — new bismuth minerals occurrence. Ore Geol. Rev. 65, 132–147.

Buzgar, N., Buzatu, A., Sanislav, I.V., 2009. The Raman study on certain sulfates. An. St. Univ. Al. I. Cuza Iasi Geol. LV-1, 5–23.

Chio, C.H., Sharma, S.K., Muenow, D.W., 2005. Micro-Raman studies of hydrous ferrous sulfates and jarosites. Spectrochim. Acta A Mol. Biomol. Spectrosc. 61, 2428–2433.

Chio, C.H., Sharma, S.K., Muenow, D.W., 2007. The hydrates and deuterates of ferrous sulfate (FeSO4): a Raman spectroscopic study. J. Raman Spectrosc. 38, 87–99.

Chou, I.M., Seal, R.R., Wang, A., 2013. The stability of sulfate and hydrated sulfate minerals near ambient conditions and their significance in environmental and planetary sciences. J. Asian Earth Sci. 62, 734–758.

Cloutis, E., Hawthorne, F., Mertzman, S., Krenn, K., Craig, M., Marcino, D., Methot, M., Strong, J., Mustard, J., Blaney, D., 2006. Detection and discrimination of sulfate minerals using reflectance spectroscopy. Icarus 184, 121–157.

Croitoru, A.-E., Piticar, A., 2013. Changes in daily extreme temperatures in the extra-Carpathians regions of Romania. Int. J. Climatol. 33, 1987–2001.

Croitoru, A.-E., Piticar, A., 2014. Changes in Hot Extreme Temperature Indices in Carpathian and Intra-Carpathian Areas of Romania. 14th International Multidisciplinary Scientific GeoConference SGEM 2014, Conference Proceedings 2. pp. 305–312.

Croitoru, A.-E., Piticar, A., Burada, D.C., 2015. Changes in Precipitation Extremes in Romania. Article In Press, Corrected Proof, Quatern. Int.

Damian, G., Damian, F., Cook, N.J., Ciobanu, C.L., 2003. Ag-sulphosalts in upper parts of the Baia Sprie deposit (Romania): microanalyses and implications for the deposit zonality. Studia Universitatis Babes-Bolyai, Geologia, pp. 37–39.

Dill, H.G., Bosse, H.R., Kassbohm, J., 2000. Mineralogical and chemical studies of volcanic-related argillaceous industrial minerals of the central American Cordillera (Western El Salvador). Econ. Geol. 95, 517–538.

Dill, H.G., Weber, B., Botz, R., 2013. Metalliferous duricrusts ("orecretes") — markers of weathering: a mineralogical and climatic-geomorphological approach to supergene Pb-Zn-Cu-Sb-P mineralization on different parent materials. Neus. Jb. Miner. Abh. 190, 123–195.

Dragotă, C.S., Kucsicsa, G., 2011. Global climate change-related particulaties in the Rodnei Mountains National Park. Carpath. J. Earth Environ. Sci. 6, 43–50.

Dumitrescu, A., Birsan, M.-V., 2015. ROCADA: a gridded daily climatic dataset over Romania (1961–2013) for nine meteorological variables. Nat. Hazards 78, 1045–1063.

Falgayrac, G., Sobanska, S., Brémard, C., 2014. Raman diagnostic of the reactivity between $ZnSO_4$ and $CaCO_3$ particles in humid air relevant to heterogeneous zinc chemistry in atmosphere. Atmos. Environ. 85, 83–91.

Frost, R.L., 2011. A Raman spectroscopic study of copiapites $Fe_2 + Fe_3 + (SO_4)_6(OH)_2 \cdot 20H_2O$: environmental implications. J. Raman Spectrosc. 42, 1130–1134.

Frost, R.L., Gobac, Ž.Ž., López, A., Xi, Y., Scholz, R., Lana, C., Lima, R.M.F., 2014. Characterization of the sulphate mineral coquimbite, a secondary iron sulphate from Javier

Ortega mine, Lucanas Province, Peru — using infrared, Raman spectroscopy and thermogravimetry. J. Mol. Struct. 1063, 251–258.
Garratt, J.R., 1992. Extreme maximum land surface temperatures. J. Appl. Meteor. 31, 1096–1105.
Grancea, L., Bailly, L., Leroy, J., Banks, D., Marcoux, E., Milesi, J.P., Cuney, M., Andre, A.S., Iştvan, D., Fabre, C., 2002. Fluid evolution in the Baia Mare epithermal gold/polymetallic district, Inner Carpathians, Romania. Mineral. Deposita 37, 630–647.
Hawthorne, F.C., Krivovichev, S.V., Burns, P.C., 2000. The crystal chemistry of sulfate minerals, in: Alpers, C.N., Jambor, J.L., Nordstrom, D.K. (Eds.), Sulfate Minerals — Crystallography, Geochemistry, and Environmental Significance. Reviews in Mineralogy and Geochemistry, Mineralogical Society of America and Geochemical Society, Washington, pp. 1–112.
Herb, W.R., Janke, B., Mohseni, O., Stefan, H.G., 2008. Ground surface temperature simulation for different land covers. J. Hydrol. 356, 327–343.
Jambor, J.L., Nordstrom, D.K., Alpers, C.N., 2000. Metal-sulfate salts from sulfide mineral oxidation, in: Alpers, C.N., Jambor, J.L., Nordstrom, D.K. (Eds.), Sulfate Minerals — Crystallography, Geochemistry, and Environmental Significance. Reviews in Mineralogy and Geochemistry, Mineralogical Society of America and Geochemical Society, Washington, pp. 305–350.
Joeckel, R.M., Ang Clement, B.J., VanFleet Bates, L.R., 2005. Sulfate-mineral crusts from pyrite weathering and acid rock drainage in the Dakota Formation and Graneros Shale, Jefferson County. Nebraska. Chem. Geol. 215, 433–452.
Kong, W.G., Wang, A., Freeman, J.J., Sobron, P., 2011. A comprehensive spectroscopic study of synthetic Fe^{2+}, Fe^{3+}, Mg^{2+} and Al^{3+} copiapite by Raman, XRD, LIBS, MIR and vis-NIR. J. Raman Spectrosc. 42, 1120–1129.
Koppen, W., 1936. Das geographisca system der klimate. In: Koppen, W., Geiger, G.C. (Eds.), Handbuch der Klimatologie. Gebr, Borntraeger, pp. 1–44.
Lane, M.D., 2007. Mid-infrared emission spectroscopy of sulfate and sulfate-bearing minerals. Am. Mineral. 92, 1–18.
Lemus, R., 2004. Vibrational excitations in H_2O in the framework of a local model. J. Mol. Spectrosc. 225, 73–92.
Ling, Z.C., Wang, A., 2010. A systematic spectroscopic study of eight hydrous ferric sulfates relevant to Mars. Icarus 209, 422–433.
Majzlan, J., Alpers, C.N., Koch, C.B., McCleskey, R.B., Myneni, S.C.B., Neil, J.M., 2011. Vibrational, X-ray absorption, and Mössbauer spectra of sulfate minerals from the weathered massive sulfide deposit at Iron Mountain California. Chem. Geol. 284, 296–305.
Manilici, V., Giuşcă, D., Stiopol, V., 1965. Study of Baia Sprie ore Deposit (in Romanian). Memoriile Comitetului Geologic, Institutul Geologic Bucuresti VII, pp. 1–95.
Nakamoto, K., 2009. Infrared and Raman Spectra of Inorganic and Coordination Compounds Part A: Theory and Applications in Inorganic Chemistry (Sixth edition). John Wiley and Sons, New Jersey.
NMA, 2015. The National Meteorological Administration — Precipitations archive. unpublished data, Romania.
Omori, K., 1968. Infrared diffraction and the far infrared spectra of anhydrous sulfates. Mineral. J. 5, 334–354.
Peel, M.C., Finlayson, B.L., McMahon, T.A., 2007. Updated world map of the Köppen–Geiger climate classification. Hydrol. Earth Syst. Sc. 11, 1633–1644.
Piticar, A., Ristoiu, D., 2012. Analysis of air temperature evolution in northeastern Romania and evidence of warming trend. Carpath. J. Earth Environ. Sci. 7, 97–106.
Rudolph, W.W., Brooker, M.H., Tremaine, P.R., 1999. Raman spectroscopy of aqueous $ZnSO_4$ solutions under hydrothermal conditions: solubility, hydrolysis, and sulfate ion pairing. J. Solut. Chem. 28, 621–630.
Schaider, L.A., Senn, D.B., Estes, E.R., Brabander, D.J., Shine, J.P., 2014. Sources and fates of heavy metals in a mining-impacted stream: temporal variability and the role of iron oxides. Sci. Total Environ. 490, 456–466.
Seal, R.R., Alpers, C.N., Rye, R.O., 2000. Stable isotope systematics of sulfate minerals, in: Alpers, C.N., Jambor, J.L., Nordstrom, D.K. (Eds.), Sulfate Minerals — Crystallography, Geochemistry, and Environmental Significance. Reviews in Mineralogy and Geochemistry, Mineralogical Society of America and Geochemical Society, Washington, pp. 541–593.
Seghedi, I., Downes, H., Szakács, A., Mason, P., Thirwall, M.T., Roşu, E., Pécskay, Z., Márton, E., Panaiotu, C., 2004. Neogene–Quaternary magmatism and geodynamics in the Carpathian–Pannonian region: a synthesis. Lithos 72, 117–146.
Stanciu, C., 1973. Hydrothermal transformation processes in Herja and Baia Sprie ore deposits — Gutîi Mountains (in Romanian). Institutul Geologic, Studii tehnice şi economice 9, 73–94.
Summerfield, M.A., 1991. Global Geomorphology. John Wiley and Sons Inc., New York.
Valente, T.M., Gomes, C.L., 2009. Occurrence, properties and pollution potential of environmental minerals in acid mine drainage. Sci. Total Environ. 407, 1135–1152.
Valente, T.M., Antunes, M., Sequeira Braga, A., Prudêncio, M.I., Marques, R., Pamplona, J., 2011. Mineralogical attenuation for metallic remediation in a passive system for mine water treatment. Environ. Earth Sci. 66, 39–54.
Valente, T., Grande, J.A., de la Torre, M.L., Santisteban, M., Cerón, J.C., 2013. Mineralogy and environmental relevance of AMD-precipitates from the Tharsis mines, Iberian Pyrite Belt (SW, Spain). Appl. Geochem. 39, 11–25.
Velasco, F., Alvaro, A., Suarez, S., Herrero, J.-M., Yusta, I., 2005. Mapping Fe-bearing hydrated sulphate minerals with short wave infrared (SWIR) spectral analysis at San Miguel mine environment, Iberian Pyrite Belt (SW Spain). J. Geochem. Explor. 87, 45–72.
Wang, A., Zhou, Y., 2014. Experimental comparison of the pathways and rates of the dehydration of Al-, Fe-, Mg- and Ca-sulfates under Mars relevant conditions. Icarus 234, 162–173.
Yilmaz, H., Toy, S., Irmak, M.A., Yilmaz, S., Bulut, Y., 2008. Determination of temperature differences between asphalt concrete, soil and grass surfaces of the city of Erzurum, Turkey. Atmósfera 21, 135–146.